

**Fermi National Accelerator Laboratory**

**FERMILAB-Conf-96/454-E**

**DØ and CDF**

## **Recent Results from the Fermilab Tevatron**

N.A. Graf

For the DØ and CDF Collaborations

*Brookhaven National Laboratory  
P.O. Box 5000, Upton, New York 11793-5000*

*Fermi National Accelerator Laboratory  
P.O. Box 500, Batavia, Illinois 60510*

January 1997

Presented at the *Standard Model and Beyond (SMAB)*, Georgia, CIS, August 4-10, 1996

## **Disclaimer**

*This report was prepared as an account of work sponsored by an agency of the United States Government. Neither the United States Government nor any agency thereof, nor any of their employees, makes any warranty, expressed or implied, or assumes any legal liability or responsibility for the accuracy, completeness, or usefulness of any information, apparatus, product, or process disclosed, or represents that its use would not infringe privately owned rights. Reference herein to any specific commercial product, process, or service by trade name, trademark, manufacturer, or otherwise, does not necessarily constitute or imply its endorsement, recommendation, or favoring by the United States Government or any agency thereof. The views and opinions of authors expressed herein do not necessarily state or reflect those of the United States Government or any agency thereof.*

## **Distribution**

*Approved for public release; further dissemination unlimited.*

# RECENT RESULTS FROM THE FERMILAB TEVATRON

**N.A. GRAF<sup>1</sup>**

*Brookhaven National Laboratory*

*P.O. Box 5000 Upton, New York 11973-5000*

*USA*

## **Abstract**

This talk is intended to present a brief overview of selected physics analyses being conducted at Fermilab's Tevatron collider. Selected topics from electroweak and top analyses being conducted by DØ and CDF will be presented to give a flavor of the rich variety of physics currently being studied at the Tevatron.

## **1 Introduction**

The DØ and CDF experiments use large multi-purpose detectors to exploit the rich menu of physics produced by the high energy proton-antiproton collisions at Fermilab's Tevatron. The analyses presented here were selected from the large number of topics currently being studied in the data samples accumulated during the period 1992-1996 and representing in excess of  $100 \text{ pb}^{-1}$  per experiment. The very large data sets arising from such high integrated luminosities provide very high statistics samples of W and Z bosons, allowing precision tests of the Standard Model to be carried out. In addition, this data sample has allowed the top quark to finally be discovered. In this talk, measurements of the top quark production cross section and top quark mass are presented.

Clearly in a talk of this length not all topics can be discussed, nor can analyses be presented in any great detail. It is intended to be a general description for an audience composed of both students and physicists not necessarily expert in these fields.

## **2 The Tevatron**

Fermi National Accelerator Laboratory is located near Chicago in the USA and is home to the world's highest energy particle accelerator, the 1 kilometer radius Tevatron. The Tevatron provides experimentalists with proton antiproton ( $\bar{p}p$ ) collisions at a center of mass energy of 1.8 TeV with delivered luminosities of  $\sim 10^{31} \text{ cm}^{-2} \text{ s}^{-1}$ . The DØ and CDF detectors are housed in two of the interaction regions, with a gaussian luminous region with  $\sigma \sim 30 \text{ cm}$  along the beam and beam profiles  $\sim 40 \mu\text{m}$  in the transverse dimension. The time between crossings of the bunches is  $3.5 \mu\text{sec}$ . Figure 1 is a sketch showing the locations of the accelerators and detectors.

---

<sup>1</sup>E-mail address: ngraf@fnal.gov

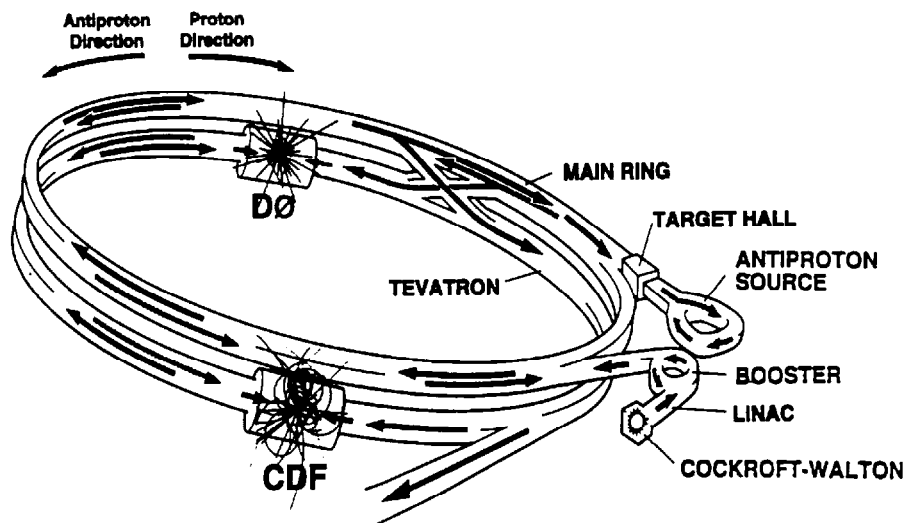


Figure 1: The Fermilab accelerators and collider detectors.

### 3 The Collider Detectors

The  $D\bar{0}$  and CDF [1] experiments utilize large multi-purpose detectors composed of many subsystems to detect the myriad final-state products arising for  $\bar{p}p$  annihilations. Both detectors employ drift chambers to track charged particles from the interaction region to the calorimeter. The CDF detector has enjoyed the advantage of an upgraded silicon vertex detector which provides very high resolution tracking near the vertex. Both detectors have massive segmented calorimeters to contain and measure the energies of electromagnetic and hadronic showers, outside of which are additional drift chambers to detect the passage of muons, which escape the calorimeter. The analyses which follow are based on event reconstructions employing jets, electrons, muons and neutrinos. (Tau leptons are reconstructed in the collider environment only with great difficulty due to the large hadronic backgrounds.) Brief descriptions of the particle identification algorithms are presented here for completeness.

Jets are reconstructed in both detectors by clustering energy depositions in the calorimeters using a fixed cone algorithm. Corrections are then applied to account for losses outside the cone as well as for nonlinearities in the detectors' low energy response and leakage into the cone from the underlying event and multiple interactions in the same beam crossing.

Both experiments identify electrons by detecting their isolated electromagnetic showers in the calorimeters. The longitudinal and lateral developments of these showers are required to be consistent with expectations from testbeam measurements and Monte Carlo simulations. Additionally, tracks in the central tracking volume are required to point to the shower. CDF further insists that the momentum of the track match the energy of the EM cluster, whereas  $D\bar{0}$  uses the ionization along the track and information gathered from a Transition Radiation Detector (TRD) in the central region to provide additional confirmation.

Muons, interacting only minimally in the calorimeters, are detected in the outer muon chambers. In CDF, the muon momentum is derived from the matching inner central track, whereas in DØ the momentum is measured in the toroidal field of the outer muon magnetic system.

The presence of neutrinos is inferred from an imbalance in the transverse energy distribution derived by vectorially summing the calorimeter energy depositions and accounting for muons. Since initially the proton-antiproton system has only minimal transverse momentum any final imbalance must be due to mismeasurement arising from detector resolution or inhomogeneities or to undetected particles. However, only information about the transverse energy of the neutrino can be inferred by this method, no information about the longitudinal momentum is available.

## 4 The Physics Menu

There are many analyses being conducted at DØ and CDF which could have been presented at a conference entitled “Standard Model and Beyond”: analyses of jet production which go beyond simple “tests of QCD (Quantum Chromodynamics)” and which actually provide strong constraints on Next-to-Leading-Order (NLO) calculations are being undertaken; the physics of b quark production and decay are being vigorously pursued; signatures of Supersymmetry (SUSY) as well as other new phenomena are being searched for. This article is restricted to the results of only a few analyses in the electroweak and top quark sectors. The one provides precision measurements of the intermediate vector bosons ( $W^\pm, Z^0$ ), whereas the other provides updated information on the newly discovered sixth quark. Combined, the two topics can be used to constrain the as yet unexplored Higgs sector of the Standard Model.

## 5 Electroweak Physics

Although the intermediate vector bosons decay predominantly into pairs of quarks, they are detected in both CDF and DØ through their leptonic decays. This is due to the overwhelming production of dijet events through ordinary QCD and the impossibility of uniquely identifying dijet final states as arising from W or Z boson decays. The final state leptons are characterized by high momenta and tend to be quite isolated from other activity in the event. Z bosons are detected by identifying pairs of high transverse momentum ( $E_T$ ) electrons or muons (taus are not uniquely identified, nor are neutrinos individually detectable). The invariant mass of the Z can then be reconstructed, giving rise to a peak at the Z mass in the invariant mass distribution. The purity of the sample can be directly determined by measuring the number of events which lie outside the peak region (and after accounting for the Drell-Yan continuum production of dilepton events). Figure 2a shows the dielectron invariant mass spectrum measured at DØ from the Run 1b data sample.

W bosons are detected by their decay into a lepton and its associated neutrino. Since no information is available about the longitudinal momentum of the neutrino, only so-called “transverse” properties of the W boson can be directly measured. The final-state signature of a W boson decay consists of a high  $E_T$  electron or muon and a significant

amount of missing transverse energy. From this information, the transverse mass ( $M_T$ ), which is the two-dimensional analogue of the invariant mass is reconstructed as  $M_T = \sqrt{2E_T^e E_T^{\nu}(1 - \cos\phi^{e\nu})}$ . This distribution exhibits a sharp Jacobian peak at roughly the mass of the W boson, with a tail extending down to lower masses. There is, however, no explicit analytic form for this distribution. Figure 2b shows the  $e\nu$  transverse mass spectrum for W boson candidate events as measured at DØ from the Run 1b data sample.

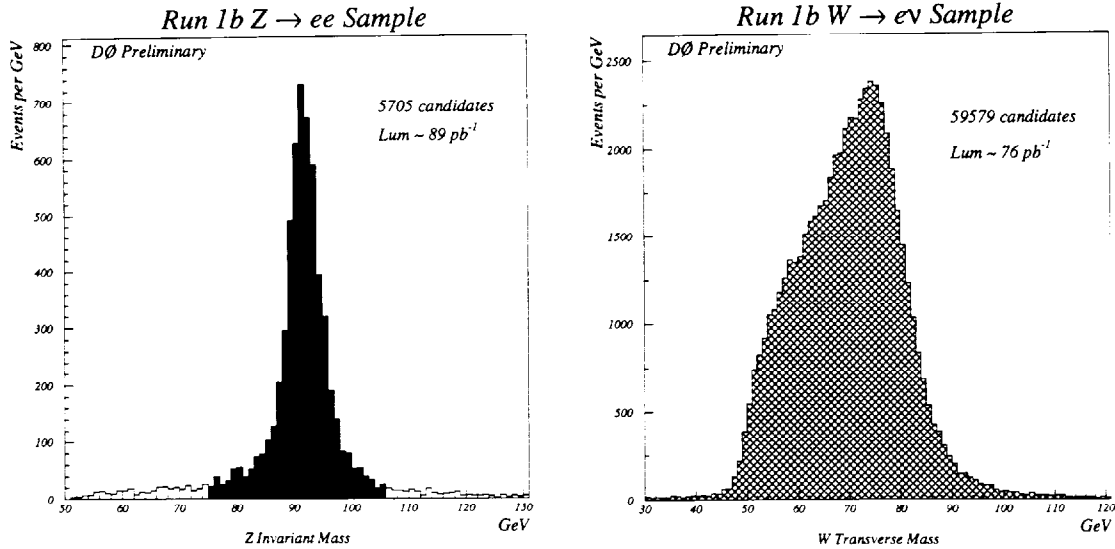


Figure 2: The dielectron invariant mass distribution (left) and the transverse mass distribution for  $W \rightarrow e\nu_e$  candidates at DØ .

## 5.1 W and Z Cross Sections

The cross sections for W and Z boson production at the Tevatron are measured indirectly through the cross section times branching ratio into leptons. This measurement provides not only a comparison to theoretical predictions, but also provides a method to indirectly measure the total width of the W boson, thereby providing information on all of its decay channels. As can be seen from Table 1 [2, 3], the direct measurements of the W and Z boson production cross sections are dominated by the systematic uncertainties of the detector acceptances and efficiencies as well as the integrated luminosity. Additionally, the theoretical predictions are limited by the precision with which the parton distribution functions (pdf's) are known. However, by taking the ratio of W to Z boson cross sections, many of these systematic uncertainties disappear or are largely cancelled. Additionally, information about the inclusive width of the W boson can be derived from this ratio. Comparing the experimentally measured value of the width to that predicted by the Standard Model can shed light on any non-standard decays of the W boson, since any additional decay modes will lead to an increase in the W width. Theoretically, the ratio R can be expressed as a

	$\sigma_W \cdot B(W \rightarrow \ell\nu)nb$	$\sigma_Z \cdot B(Z \rightarrow \ell\ell)nb$
DØ (e)	$2.38 \pm 0.01 \pm 0.22$	$0.235 \pm 0.003 \pm 0.021$
DØ ( $\mu$ )	$2.28 \pm 0.04 \pm 0.25$	$0.202 \pm 0.016 \pm 0.026$
CDF (e)	$2.49 \pm 0.02 \pm 0.12$	$0.231 \pm 0.001 \pm 0.011$
CDF ( $\mu$ )	$2.48 \pm 0.03 \pm 0.16$	$0.203 \pm 0.010 \pm 0.012$
Standard Model	$2.42^{+0.13}_{-0.11}$	$0.226^{+0.011}_{-0.009}$

Table 1: W and Z production cross sections times leptonic branching ratios. The first uncertainties are statistical only, the second include systematic uncertainties arising from the detector efficiencies and acceptances as well as the luminosity measurement.

combination of factors which are either well measured or precisely calculable as follows:

$$R_\ell = \frac{\sigma \cdot B(W \rightarrow \ell\nu)}{\sigma \cdot B(Z \rightarrow \ell\ell)} = \frac{\sigma_W}{\sigma_Z} \cdot \frac{\Gamma(Z)}{\Gamma(Z \rightarrow \ell\ell)} \cdot \frac{\Gamma(W \rightarrow \ell\nu)}{\Gamma(W)}$$

Combining the published ratios of W and Z cross sections for the two experiments results in a value of  $R = 10.90 \pm 0.32$ , from which one derives a value for the W width of  $\Gamma_W = 2.043 \pm 0.062$  GeV. Comparing this to the Standard Model prediction of  $\Gamma_W = 2.077 \pm 0.014$  GeV allows one to set a 95% confidence level upper limit of  $\Gamma < 109$  MeV on non-Standard Model decays of the W.

A direct measurement of the W width has been conducted at CDF by measuring the high end of the transverse mass distribution and comparing it to that derived from a Monte Carlo simulation [4]. The value of  $\Gamma_W = 2.11 \pm 0.32$  GeV is less precise, but in good agreement with the value extracted from the ratio of cross sections.

## 5.2 The W mass

Precision measurements of the W mass provide strong constraints on the Standard Model. The W mass is sensitive to radiative corrections involving the top quark and Higgs masses. Therefore, combined with the top quark mass, a precision measurement of the W boson mass provides information and constraints on the Higgs sector. Alternatively, deviations from predictions may point to physics beyond the Standard Model. As mentioned previously, W bosons are detected by their decays into electrons and muons and their associated neutrinos. Since the neutrino's longitudinal momentum is not derivable, the W boson mass must be extracted from transverse quantities. In this presentation, only mass determinations extracted from the transverse mass will be presented, although one could utilize the electron or muon transverse momentum, or the missing transverse energy in the event to determine the mass. Unlike the invariant mass, no analytic form for the transverse mass is available, so strong reliance is made on Monte Carlo simulation of the detectors to various hypothetical input W masses.

CDF measures the W boson mass using both electron and muon final states. The absolute momentum scale of the CTC is calibrated using a large sample of  $J/\psi \rightarrow \mu^+ \mu^-$

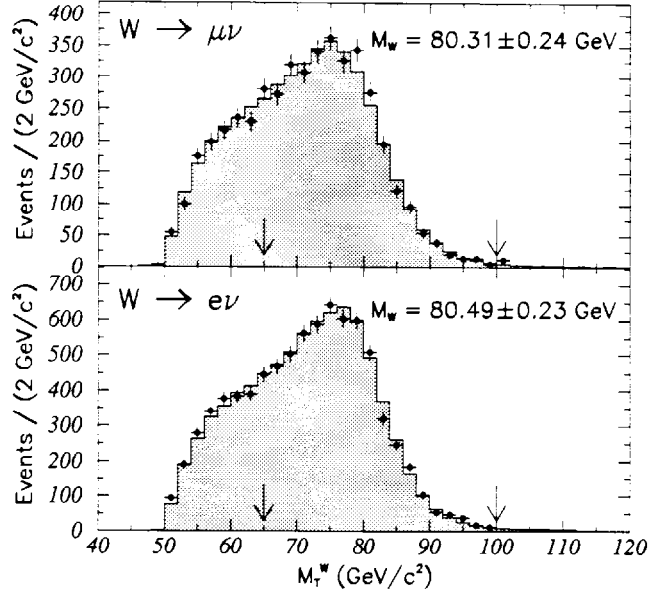


Figure 3: The transverse mass distributions for W boson decays into muons (upper) and electrons (lower) as measured by CDF from the Run 1a data sample, as well as results of the fits.

events and checked at the  $\Upsilon$  and Z boson resonances. This calibration is then transferred to the calorimeter by matching the energies of electromagnetic clusters to the momentum of the associated electron track in the CTC, accounting for energy losses in the material in the beam pipe and tracking system.

DØ measures the W boson mass indirectly, using only electron final states, by experimentally determining the ratio of W boson mass to Z boson mass and then applying this ratio to the well-determined Z boson mass measured at LEP. Testbeam measurements of the energy response of the DØ calorimeter provide strong evidence for a linear relationship between observed and true energy. The scale and offset of the calorimeter response is set by analyzing Z boson and  $J/\psi$  decays to electrons as well as reconstructing  $\pi^0$  decays in the central calorimeter.

The detector response to both the W boson decay products and the recoiling hadronic system, including efficiencies and resolutions, is modeled from the data itself. Additionally, the effect of the underlying event and of multiple interactions is simulated by using real data events overlapped onto the simulated events. Transverse mass line shapes are then generated by simulating the response to millions of Monte Carlo events generated at various values of the W boson mass. Maximum likelihood fits are then performed to the data and Monte Carlo spectra. DØ repeats the process for Z bosons to extract the mass ratio. A full accounting of the systematic uncertainties in these measurements lies outside the scope of this article. Full details are available in the references.

The transverse mass distributions for the muon and electron decay channels of the W boson as measured by CDF [5] for their Run 1a data sample ( $\int \mathcal{L} \approx 20 \text{ pb}^{-1}$ ) are shown in

Figure 3. The measured values are:

$$M_W(\mu\nu) = 80.310 \pm 0.205(stat) \pm 0.130(syst) GeV,$$

$$M_W(e\nu) = 80.490 \pm 0.145(stat) \pm 0.175(syst) GeV.$$

The DØ experiment has analyzed its data from the Run 1a [6] and 1b (preliminary) [8] periods separately and has measured the following values:

$$M_W(1a) = 80.35 \pm 0.14(stat) \pm 0.23(syst) GeV,$$

$$M_W(1b) = 80.38 \pm 0.07(stat) \pm 0.15(syst) GeV.$$

The measured values are seen to be in good agreement with one another. Combining the values together with the previous measurement by the UA2 experiment [7], and taking into account correlations in the uncertainties, yields a current (preliminary) value for the W boson mass of:

$$M_W \text{ (world preliminary)} = 80.35 \pm 0.13 GeV.$$

### 5.3 Production properties

Uncertainties in the parton distribution functions within the proton contribute rather substantially to the uncertainties in many of the electroweak measurements undertaken at the Tevatron. Constraints on these distributions can be extracted from the lepton charge asymmetry arising from W boson decays. In  $\bar{p}p$  annihilations,  $W^+(W^-)$  bosons are produced

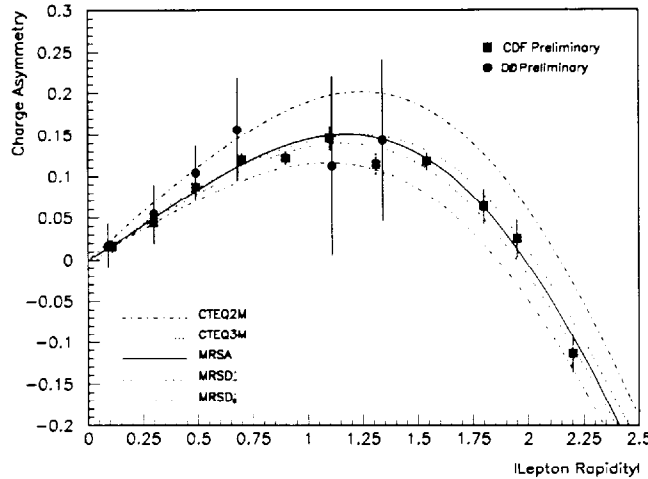


Figure 4: The lepton charge asymmetry vs. rapidity for W events.

mainly from  $u\bar{d}(d\bar{u})$  quark pairs. Due to the stiffer momentum distribution of u quarks in the proton compared to d quarks,  $W^+(W^-)$  bosons tend to be boosted along the proton (antiproton) direction. The decay products of the W boson are then distributed according to the well-known V-A coupling and tend to be boosted in the same direction as the boson itself. Therefore, by measuring the asymmetry in the charged lepton distributions arising from W decays, one can gain information about the u and d quark pdf ratios. The asymmetry is defined as:

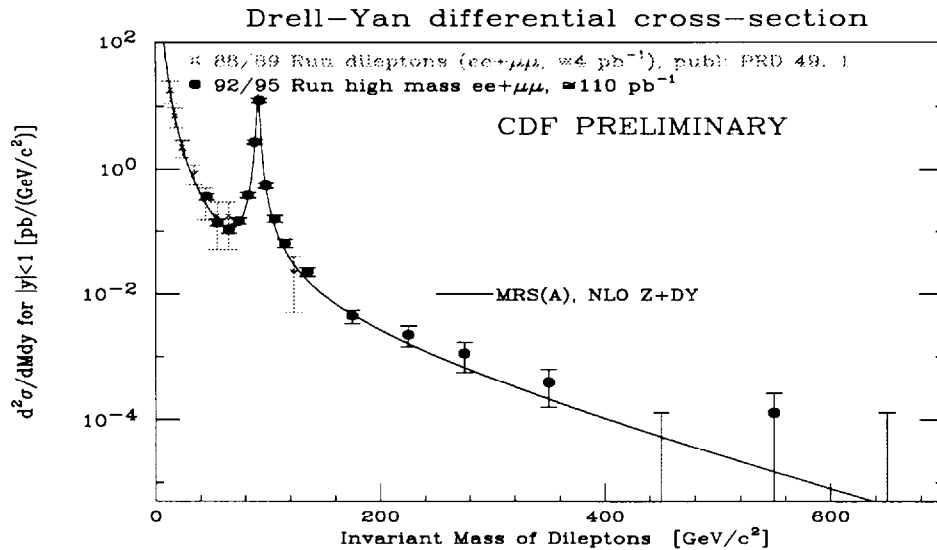


Figure 5: The Drell-Yan ( $ee + \mu\mu$ ) differential cross section  $d^2\sigma/dMdy$  as measured by CDF.

$$A(\eta) = \frac{N^+(\eta) - N^-(\eta)}{N^+(\eta) + N^-(\eta)}$$

where  $N^+(\eta)$  is the number of events with a positive lepton in a positive region, or a negative lepton in a negative region (positive correlation), and  $N^-(\eta)$  is defined conversely (negative correlation). Figure 4 shows the measured lepton charge asymmetry versus the charged lepton's rapidity for CDF (electrons and muons) [9] and DØ (muons only). The most recent pdf fits now include the published CDF data.

CDF has complemented their previously published [10] Drell-Yan differential cross section with a preliminary analysis of their Run 1 data. The vastly improved statistics ( $\simeq 110pb^{-1}$  vs  $\simeq 4pb^{-1}$ ) have greatly extended the reach of this measurement as is shown in Figure 5 which presents the differential cross section  $d^2\sigma/dMdy$  for  $ee$  and  $\mu\mu$  events detected in the central rapidity interval  $|y| < 1$ . The new data agree well with the previous measurement as well as being in very good agreement with Next-to-Leading Order QCD predictions. The existence of an additional contact term interaction between quarks and leptons would affect the shape of the dilepton invariant mass distribution. Assuming a contact interaction of the form proposed in Reference [11] CDF has placed preliminary limits on this compositeness scale  $\Lambda^{-(+)} > 2.5(3.8)TeV$ , where  $\Lambda^{-(+)}$  correspond to constructive or destructive couplings, respectively. These compositeness scale limits probe distances on the order of  $10^{-17}$  cm. The forward-backward asymmetry ( $A_{FB}$ ) of dielectron production has also been measured by CDF at and above the Z boson mass, and is shown in Figure 5. The preliminary values are  $A_{FB} = 0.070 \pm 0.015(stat) \pm 0.004(sys)$  at the  $Z^0$  pole ( $75 < M_{ee} < 105GeV$ ) and  $A_{FB} = 0.43 \pm 0.08(stat) \pm 0.06(sys)$  above, again in very good agreement with the Standard Model predictions of  $0.054 \pm 0.001$  and  $0.528 \pm 0.006$ , respectively.

## 5.4 Trilinear Gauge Boson Couplings

Trilinear gauge boson couplings are couplings between the W and Z bosons and photons and are a direct consequence of the non-Abelian  $SU(2) \times U(1)$  gauge symmetry. Due to the very sensitive nature of the gauge cancellations, anomalous couplings, representing perhaps substructure of the W and Z, would manifest themselves as enhancements in the cross section for associated boson production ( $\bar{p}p \rightarrow WW, WZ, W\gamma, Z\gamma$ ), as well as modifications to the differential distributions. Probing these couplings therefore provides a crucial test of the gauge structure of the electroweak interaction. A more sensitive test of the  $WW\gamma$  vertex

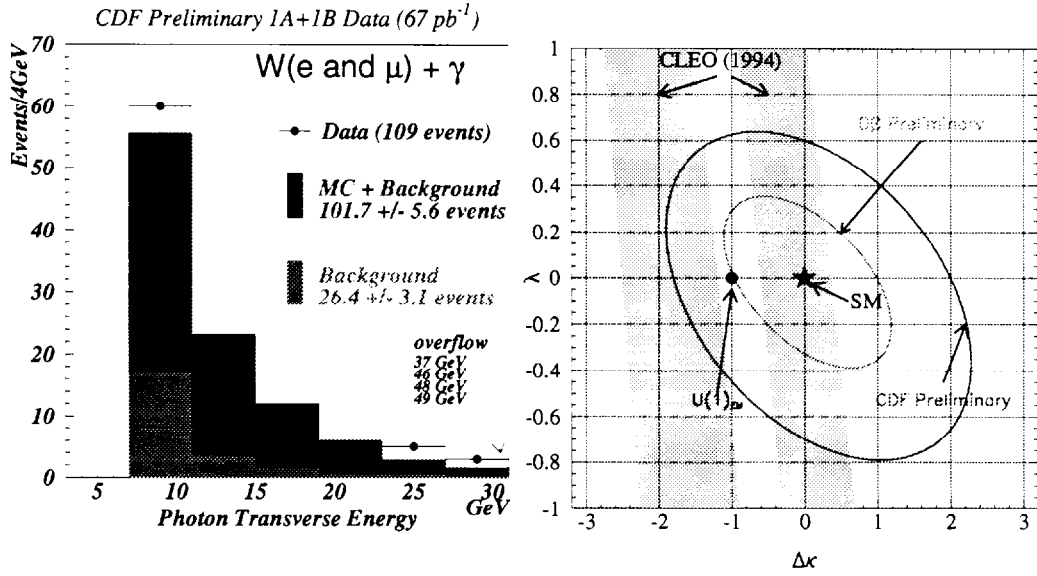


Figure 6: The photon  $E_T$  distribution as measured by CDF for  $W\gamma$  candidate events, along with expectations for the background and Standard Model contributions (left). Contour limits on the coupling parameters  $\kappa$  and  $\lambda$  at the 95% confidence level. The inner curve is the combined fit result from  $D\bar{O}$ , the outer from CDF. The shaded bands show the allowed regions from the  $b \rightarrow s\gamma$  measurement by CLEO (right).

involves a fit to the photon  $E_T$  spectrum, since anomalous couplings would give rise to significantly more high  $E_T$  photons than the Standard Model. The CP conserving coupling parameters in the Lagrangian describing the  $WW\gamma$  interaction,  $\kappa$  and  $\lambda$ , are related to the magnetic dipole moment ( $\mu_W$ ) and the electric quadrupole moment ( $Q_W$ ) via the following relations:

$$\mu_W = \frac{e}{2m_W}(1 + \kappa + \lambda); \quad Q_W = \frac{-e}{m_W^2}(\kappa - \lambda).$$

In the Standard Model  $\Delta\kappa (= \kappa - 1) = \lambda = 0$ . Both CDF and  $D\bar{O}$  have completed preliminary analyses of their Run 1 data [12] wherein events containing a high  $E_T$   $e$  or  $\mu$  and significant  $\cancel{E}_T$  (from the leptonic decay of the W boson) and a photon isolated from the lepton were selected. The photon  $E_T$  distribution was then fit to spectra generated from expected backgrounds plus Monte Carlo simulations of  $W\gamma$  production with various values of the anomalous couplings. The photon  $E_T$  distribution as measured by CDF is shown in

Figure 6. Also shown are the 95% confidence level exclusion contours from the two collider experiments as well as the results from the CLEO experiment [13]. The complementarity of the two measurements is clearly seen. The DØ collaboration has placed the following axis limits on these two couplings:  $-0.97 < \Delta\kappa < 0.99$  ( $\lambda = 0$ ) and  $-0.33 < \lambda < 0.31$  ( $\Delta\kappa = 0$ ). Analyses of the remaining channels have also been conducted [14], (the sensitivity being similar to the  $W\gamma$  channels) with the results all being consistent with Standard Model expectations.

## 6 Top Physics

Since the discovery of the top quark by the DØ and CDF collaborations in 1995 [15, 16], both experiments have added to their data samples and refined their analyses. Analyses have now shifted from a search for the top quark to measurements of its properties. This talk will concentrate on the top production cross sections and top mass measurement, but the increased statistics have also allowed new analyses to be undertaken.

### 6.1 Production cross sections

At the Tevatron, the top quark is produced predominantly in  $t\bar{t}$  pairs and, within the Standard Model, is predicted to decay almost instantaneously into a W boson and a b quark (in all analyses presented hereon it is further assumed to do so 100% of the time). The W boson then decays further, giving rise to a wide variety of final state signatures for the event, which have been loosely characterized into three classes.

“Top Dileptons” is the class of events in which both W bosons decay into either electrons or muons and their associated neutrinos (recall that taus are not easily identified at a hadron collider), giving rise to two isolated, high  $E_T$  leptons, two jets (arising from the b quarks) and considerable  $\cancel{E}_T$  from the two undetected neutrinos. CDF refers to these events as DIL (dilepton) events. The total branching fraction is roughly 5% for the three channels ( $ee, e\mu, \mu\mu$ ) with major backgrounds arising from  $W^+W^- \rightarrow l^+l^-$ , Drell-Yan production of dileptons,  $b\bar{b}, c\bar{c} \rightarrow l^+l^-$  as well as multijet events with misidentified leptons and spurious  $\cancel{E}_T$ .

“Top Lepton+Jets” includes those events in which one of the W bosons decays leptonically, the other into a  $q\bar{q}'$  pair, characterized by a single isolated, high  $E_T$  lepton, four jets (two from b quarks), and substantial  $\cancel{E}_T$  from the neutrino. These two channels ( $e$  and  $\mu$ ) comprise roughly 30% of the branching fraction with major backgrounds arising from W+multijet production as well as multijet events with misidentified leptons and spurious  $\cancel{E}_T$ . Both experiments employ methods to tag jets arising from b quarks in order to improve the signal-to-background (S/B) ratio. CDF utilizes its precision silicon vertex detector (SVX) to identify the secondary (displaced) vertices produced by the decay of long-lived b quarks. Jets arising from b quarks can also be identified by detecting low-energy leptons which are produced in semileptonic b decays. These are referred to as soft-lepton-tags (SLT) in CDF, and simply as “ $\mu$ -tagged” at DØ.

Finally, one has the “Top All Jets” sample, in which both W bosons decay hadronically, giving rise to six quark jets (two from b quarks). Although accounting for roughly 44% of the total branching fraction, this topology suffers from very severe backgrounds due to

QCD multijet production ( $S/B \sim 1/1000$ ). Strong topological cuts and the tagging of b quark jets are essential in the extraction of a signal.

Both experiments have attempted to measure the  $t\bar{t}$  production cross section in as many distinct final state channels as possible in order to glean as much information as possible out of the rather small sample of top quark events [17]. It is important not only to measure the cross section as accurately as possible, but also to provide consistency checks on the Standard Model predictions for the various channels. Tables 2 and 3 summarize the  $t\bar{t}$  production cross section as measured by the two experiments in the various channels. The measurements are all in very good agreement with the expectations for the decays of a standard model top quark as is demonstrated graphically in Figure 7. Combining the

Channel	Expected (175 GeV top)	Background	Data	$\sigma_{t\bar{t}}$ (pb) (175 GeV top)
$e\mu$	$2.0 \pm 0.3$	$0.4 \pm 0.1$	3	$4.7 \pm 3.2$
$ee$	$1.1 \pm 0.1$	$0.7 \pm 0.2$	1	
$\mu\mu$	$0.6 \pm 0.1$	$0.5 \pm 0.3$	1	
$e + jets$	$7.2 \pm 1.5$	$3.8 \pm 1.4$	10	$4.2 \pm 2.0$
$\mu + jets$	$7.2 \pm 1.7$	$5.4 \pm 2.0$	11	
$e + jets(\mu)$	$2.9 \pm 0.5$	$1.4 \pm 0.4$	5	$7.0 \pm 3.3$
$\mu + jets(\mu)$	$3.3 \pm 1.1$	$1.1 \pm 0.2$	6	
Total	$24.3 \pm 4.3$	$13.4 \pm 3.0$	37	$5.0 \pm 1.7$

Table 2: DØ  $t\bar{t}$  production cross sections.

Channel	Acceptance $\times$ Branching Ratio (%)	Background	$N_{obs}$	$\sigma_{t\bar{t}}$ (pb) (175 GeV top)
<i>SVX</i>	$3.5 \pm 0.7$	$8.0 \pm 1.4$	34	$6.8^{+2.3}_{-1.8}$
<i>SLT</i>	$1.7 \pm 0.3$	$24.3 \pm 3.5$	40	$8.0^{+4.4}_{-3.6}$
<i>DIL</i>	$0.77 \pm 0.08$	$2.1 \pm 0.4$	10	$9.3^{+4.4}_{-3.4}$
<i>DIL</i> ( $\tau$ )	$0.119 \pm 0.014$	$1.96 \pm 0.35$	4	$15.6^{+18.6}_{-13.2}$
<i>DIL</i> ( $b - Tag$ )	$0.51 \pm 0.03$	$1.4 \pm 0.3$	4	$4.6^{+4.4}_{-3.1}$
<i>All Jets</i>	$4.7 \pm 1.6$	$137.1 \pm 11.3$	192	$10.7^{+7.6}_{-4.0}$

Table 3: CDF  $t\bar{t}$  production cross sections.

dilepton (DIL) and lepton+jets channels (SVX, SLT), the CDF collaboration arrives at  $\sigma_{t\bar{t}} = 7.5^{+1.9}_{-1.6}$  pb, which is to be compared to the DØ combined value of  $\sigma_{t\bar{t}} = 5.2 \pm 1.8$  pb. The experimental measurement of  $\sigma_{t\bar{t}}$ , as well as the theoretical prediction, depends on the value of the top quark mass. This dependence is exhibited in Figure 8, which presents the

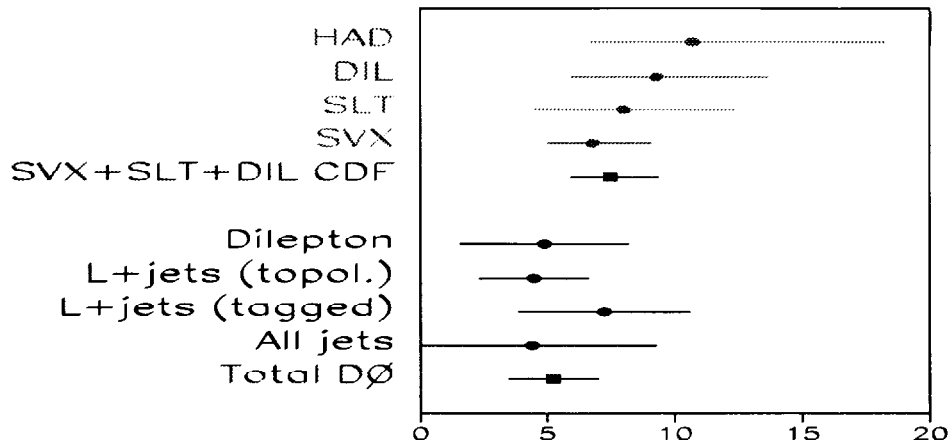


Figure 7: Summary of  $D\bar{0}$  and CDF  $t\bar{t}$  production cross section measurements.

$D\bar{0}$  and CDF preliminary measurements (evaluated at their respective values for the top quark mass), along with the theoretical predictions [19, 20, 21]. The agreement is seen to be quite good. The combined (preliminary) value for the  $t\bar{t}$  production cross section (both evaluated at a top quark mass of 175 GeV) at the Tevatron is then  $\sigma_{t\bar{t}} = 6.4^{+1.3}_{-1.2}$  pb [18].

## 6.2 The Top Mass

Although both experiments have measured the top quark mass in different channels, only the determination of the mass using the lepton+jets channels will be discussed here. Recall that this channel corresponds to the reaction  $t\bar{t} \rightarrow (Wb)(Wb) \rightarrow (\ell\nu b)(q\bar{q}'b)$ . The analysis, therefore, begins by selecting events with a high  $E_T$ , isolated electron or muon, significant  $\cancel{E}_T$ , and at least four jets in the event. One associates the four highest  $E_T$  jets on a one-to-one basis with the four quarks postulated in the event, and assumes the  $\cancel{E}_T$  is due to the neutrino from the W boson decay, giving rise to 17 measured quantities (energy and direction for the four jets and the lepton, and the two transverse components of the  $\cancel{E}_T$ ). The hypothesis adopted above provides three constraints, two from requiring two W bosons in the event (one from  $\ell\nu$ , the other from a jet-jet ( $jj$ ) pair), and one from requiring that the two top quark masses ( $\ell\nu jj$  and  $jjj$ ) be equal. The lack of knowledge of  $p_z$  of the  $\nu$  introduces a twofold ambiguity which, along with the 12 possible assignments of jets, gives rise to 24 possible solutions per event. However, in those events in which a b-jet is tagged, it is required to be assigned as a b, resulting in only 12 permutations for those events. The best mass ( $m_{fit}$ ) for each event is determined from that permutation which results in the lowest  $\chi^2$ , events which have too large a  $\chi^2$  are removed from further consideration. Since the final samples thus obtained contain few events and rather large admixtures of background events, the top quark mass is derived from a log-likelihood fit to the distributions of  $m_{fit}$ , using templates which are a combination of Monte Carlo top quark mass ( $m_{top}$ ) plus the expected

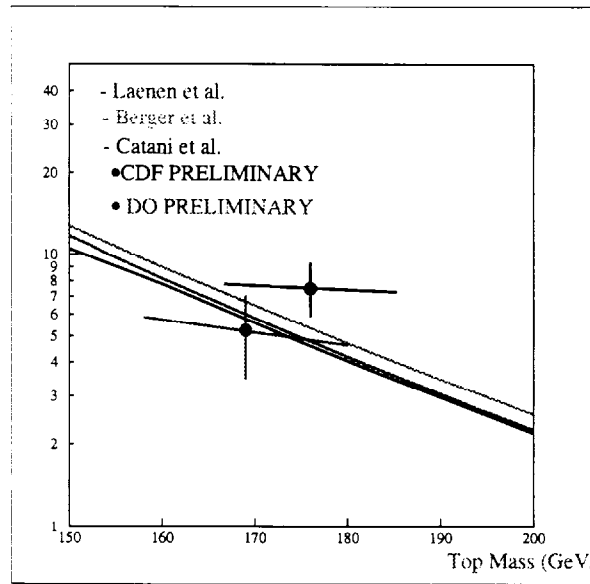


Figure 8:  $\sigma_{t\bar{t}}$  vs top quark mass. The data points represent the DØ and CDF preliminary measurements; the lines present theoretical predictions of various authors.

distribution from the background. To extract the maximum amount of information about the top quark mass without removing too many events from the final sample, both DØ and CDF have divided their data samples into exclusive subsamples with varying purity and performed fits to the data in the separate classes. This procedure makes more optimal use of the information available in each event without reducing the event sample size. CDF divides its sample into four categories in roughly ascending order of purity; untagged events, only SLT-tagged events, SVX-tagged events, and finally events with two SVX tags. CDF fits each subsample independently and combines them by taking the product of the likelihood distributions. DØ has separated its sample into six bins of varying top purity by defining a top likelihood discriminant based on the kinematic variables of the event and also on whether a jet in the event was b-tagged. (Another technique giving similar results calculates a top probability variable using a neural network.) A simultaneous fit to the full data set is then performed. By varying the input  $m_{top}$  value a log-likelihood distribution as a function of  $m_{top}$  is generated. A fit to this distribution results in the experimentally measured top quark mass, along with the statistical uncertainty in that measurement. Figure 9 shows the CDF  $m_{fit}$  distribution (solid histogram), along with predictions for the background (shaded dashed histogram) and background plus expected top signal(dashed histogram) for the best-fit top mass hypothesis. Inset is the negative log-likelihood distribution resulting from the fits to the various top quark mass hypotheses from which the top quark mass and statistical uncertainty of the fit are extracted. The corresponding plots for DØ are shown in Figure 10, with  $m_{fit}$  values represented by the histogram, along with predictions for the background (dashed points) and background plus expected top signal(solid points). A quadratic fit to the five points closest to the minimum is used to determine the top quark mass, whereas a cubic fit to the nine closest points is used to determine the uncertainty. Monte Carlo studies performed by DØ have shown a shift of 1 GeV between the input top

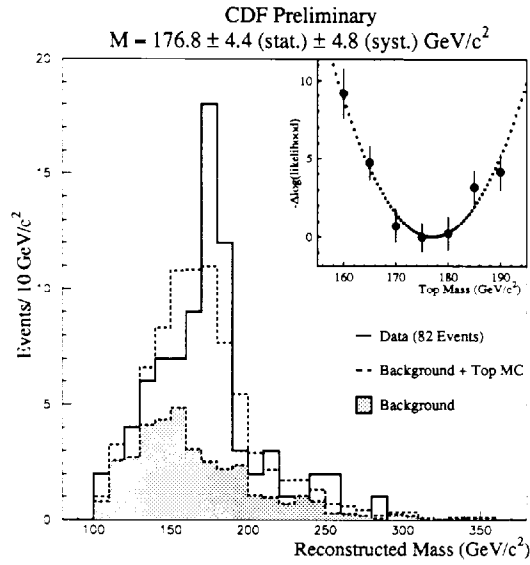


Figure 9: The CDF fit top mass distribution (solid histogram), along with predictions for the background (shaded dashed histogram) and background plus expected top signal(dashed histogram). Inset is the negative log-likelihood from which the top quark mass and statistical uncertainty of the fit are extracted.

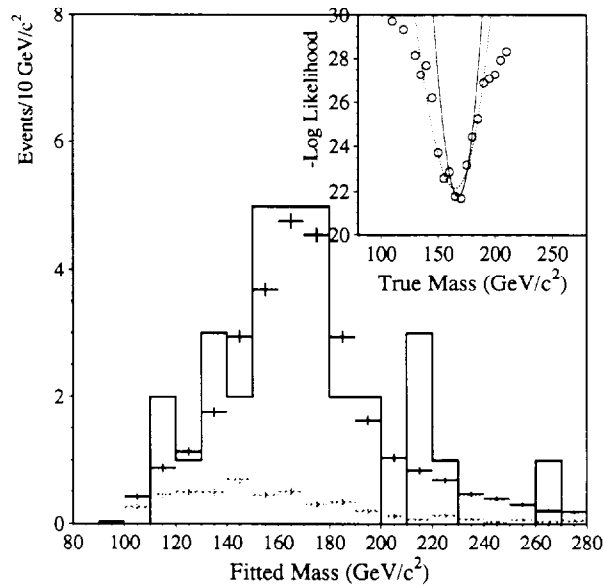


Figure 10: The DØ fit top mass distribution (histogram), along with predictions for the background (dashed points) and background plus expected top signal(solid points). Inset is the negative log-likelihood from which the top quark mass and statistical uncertainty of the fit are extracted.

quark mass and the results of fits described above. This offset is accounted for at the end of the fit procedure. The largest sources of systematic uncertainties in both experiments are the jet energy scale and uncertainties arising from initial and final state radiation, which obscure the one-to-one correspondence between jets and partons. Preliminary values for the top quark mass are then:

$$M_t(CDF) = 176.8 \pm 4.4(stat) \pm 4.8(syst) GeV,$$

$$M_t(D\emptyset) = 169 \pm 8(stat) \pm 8(syst) GeV.$$

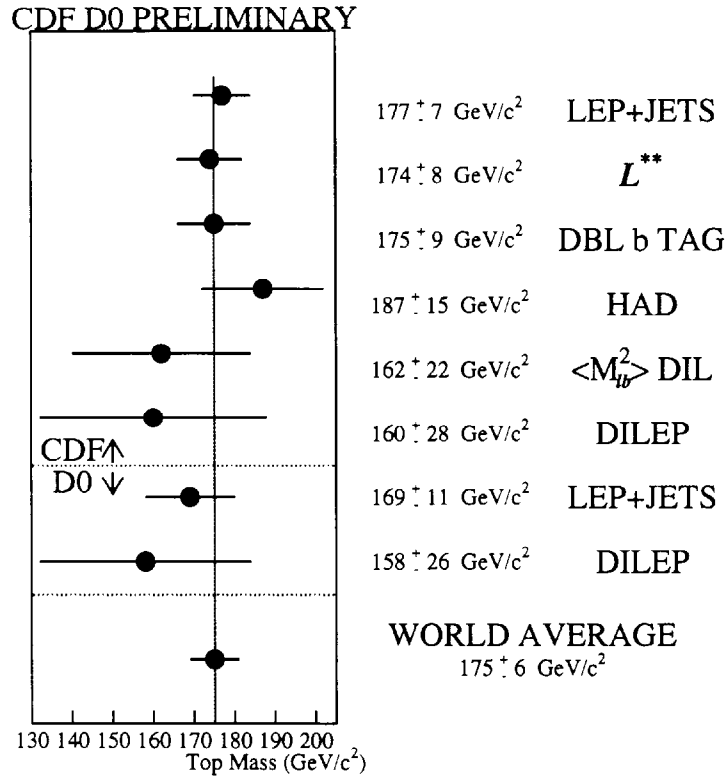


Figure 11: Summary of the DØ and CDF top quark mass measurements in the various channels. The world average value represents a combination of the DØ and CDF measurements in the lepton+jets channels only.

Although not detailed here in this writeup, measurements of the top quark mass in the other decay channels have also been conducted by both experiments, both to extract the best possible measurement and to once again double-check the consistency of the top quark hypothesis [22]. The consistency of the top quark mass determinations across the various final state subsamples is exhibited in Figure 11. The world average value represents a combination of the DØ and CDF measurements in the lepton+jets channels only and is:

$$M_t = 175 \pm 6 GeV.$$

## 7 Higgs Sector

As was mentioned in the introduction, precision measurements of the W boson and top quark mass provide constraints on the Higgs mass. Figure 12 shows the preliminary combined measurements. The Standard Model predictions for various Higgs masses are shown as bands, and the predictions from indirect electroweak measurements [23] are shown along with their  $1\sigma$  contour. Although the precision of the current measurements does not allow a definite statement to be made about the Higgs mass, the measured values are consistent with the Standard Model expectations. Final analyses of the Run 1 data are expected to reduce the uncertainty on the W boson mass measurement to 80-100 MeV, and it is anticipated that the larger data samples available from Run II will provide a measurement of the W boson mass precise to better than 50 MeV. The next run will also vastly increase the number of top quarks detected, leading to a concomitant decrease in the measurement uncertainties. Of course, Run II also provides the opportunity (albeit small) to explicitly discover the Higgs, which should not be forgotten.

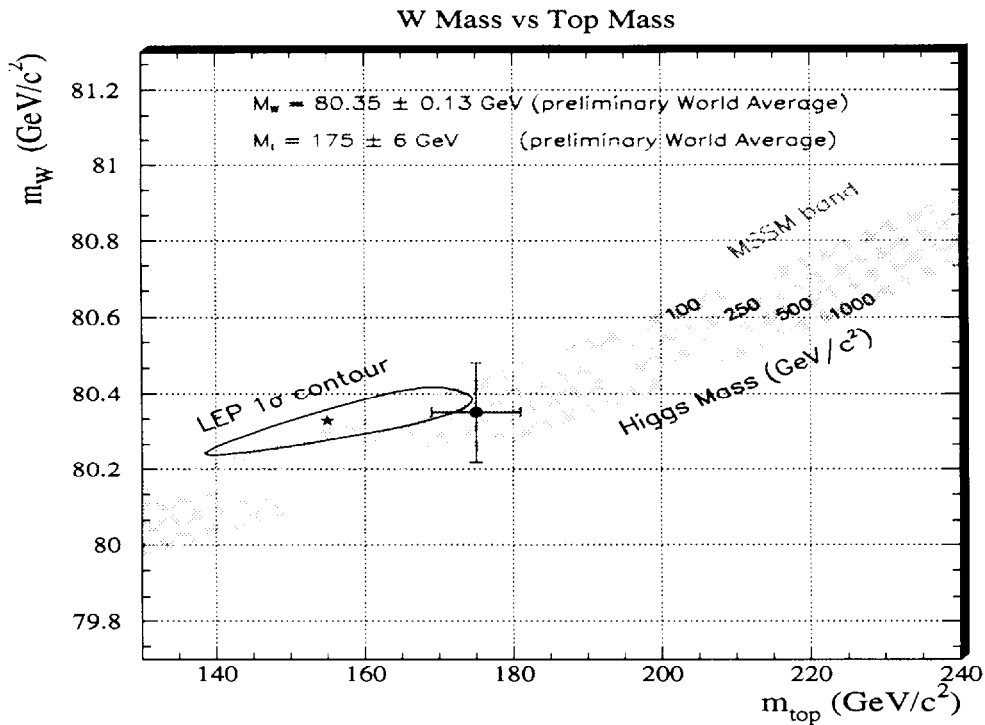


Figure 12: W boson mass vs top quark mass. Shown are the preliminary combined measurements along with the SM predictions for various values of the Higgs mass. Also shown as a contour are the predictions and  $1\sigma$  allowed values from indirect electroweak measurements.

## 8 Summary

The Tevatron has concluded a very successful Run 1, with both the DØ and CDF experiments having collected in excess of  $100\text{pb}^{-1}$  integrated luminosity of  $\bar{p}p$  collisions at  $\sqrt{s} = 1800$  GeV. In most cases preliminary analysis results have been presented and final analysis of the full data sets will reduce both the statistical and systematic uncertainties of most measurements. It should be stressed that many more analyses are underway, mining the large and very rich data samples. These include, but are not limited to QCD jet physics, B physics and searches for SUSY and other new phenomena.

In the field of electroweak physics, results have been presented on the production rates and characteristics of the inclusive production of W and Z bosons, as well as trilinear gauge boson couplings and measurements of the W boson mass. Production rates and decay characteristics of the intermediate vector bosons are in good accord with the predictions from the Standard Model, with no evidence for any nonstandard decay modes of the W boson. Searches for anomalous trilinear gauge boson couplings in several channels (*e.g.*  $W\gamma, Z\gamma, WW, WZ$ ) provide no evidence for couplings differing from their Standard Model expectations. A combined preliminary measurement of the W boson mass results in a value of  $80.35 \pm 0.13$  GeV which is not yet precise enough to constrain the Higgs mass, but it is expected that the combined error from the final analysis will be reduced to below 100MeV.

After having discovered the top quark, both collider experiments have increased the number of events in their final samples, and have improved their measurements of both the production cross sections and the top quark mass. There is now very consistent evidence for the top quark in most of its detectable decay channels, and the individual as well as inclusive production rates are in good agreement with the Standard Model predictions. A combined preliminary measurement of the top quark mass from the Tevatron is  $M_{top} = 175 \pm 6$  GeV. Although not presented, both collaborations are furthering their analyses of top quark behaviour by, for instance, searching for evidence of single top quark production and rare decays of the top quarks. Combining the results of the W boson and top quark mass analyses, one finds that the requisite precision to provide strong constraints on the Higgs mass is still lacking, but that the envelope of allowed values overlaps very well with those predicted from the Standard Model.

At the present time, both detectors are undergoing major upgrades, and the advent of the Main Injector (1999) upgrade to the Tevatron promises a substantial increase in the data available to each collaboration during Run II (a few  $\text{fb}^{-1}$ ).

There is, in conclusion, no significant disagreement between the experimental results and the predictions of the Standard Model and only the future can tell what lies beyond.

## Acknowledgments

I would like to thank the many individuals on both DØ and CDF who have assisted me in preparing this presentation, especially S. Rajagopalan, G. Snow, R. Hughes and Y-K. Kim. I extend my thanks to the NSF for its APS travel grant which made my attendance possible and to the organizers of SMAB for making the conference such an interesting experience. Both collaborations extend thanks to their funding agencies.

## References

- [1] S. Abachi *et al.*, NIM A**338** 185 (1994), F. Abe *et al.*, NIM A**271**,376 (1988).
- [2] S. Abachi *et al.*, PRL **75**, 1456 (1995), and P. Quintas in “XI Symposium Hadrons in Collisions 1996”, to be published by World Scientific.
- [3] F. Abe *et al.*, PRL **76**, 3070 (1996), and W. F. Badgett in Proceedings of the 8th DPF Meeting, August 2-6 (1994), 431, Albuquerque, New Mexico.
- [4] F. Abe *et al.*, PRL **74**, 341 (95).
- [5] F. Abe *et al.*, PRL **65**, 2243 (1990), PR **D43**, 2070 (1991); PRL **75**, 11 (1995), PR **D52**, 4784 (1995).
- [6] S. Abachi *et al.*, PRL **77**, 3309 (1996).
- [7] J. Alitti *et al.*, *Phys. Lett. B* **276**, 354 (1992).
- [8] M. Rijssenbeek (for DØ ), ICHEP’96-Warsaw Conference, FERMILAB-CONF-96/251-E.
- [9] F. Abe *et al.*, PRL **74**, 850 (1995).
- [10] F. Abe *et al.*, *Phys. Rev. D* **49**, 1 (1994).
- [11] E. Eichten *et al.*, PRL **50**, 811 (1983).
- [12] F. Abe *et al.*, PRL **74**, 1936 and 1941 (1995), S. Abachi *et al.*, PRL **74**, 1028 and 1034 (1995).
- [13] S. Playfer *et al.*, *Int. J. Mod. Phys. A***10**, 4107 (1995).
- [14] T. Yasuda (for DØ ) and L. Nodulman (for CDF), ICHEP’96 Conference Proceedings.
- [15] S. Abachi *et al.*, PRL **74**, 2632 (1995).
- [16] F. Abe *et al.*, PRL **74**, 2626 (1995).
- [17] J. Bantly (for DØ ) and A. Castro (for CDF), ICHEP’96 Conference Proceedings.
- [18] P. Tipton, ICHEP’96-Warsaw Conference Proceedings.
- [19] E. Laenen, J. Smith, and W. van Neerven, *Phys. Lett. B* **321**, 254 (1994).
- [20] E. Berger and J. Contopanagos, *Phys. Lett. B* **361**, 155 (1995), *Phys. Rev. D* **54**,3085 (1996).
- [21] S. Catani, M. Mangano, P. Nason and L. Trentadue, *Phys. Lett. B* **378**, 329 (1996).
- [22] S. Protopopescu (for DØ ) and J. Lys (for CDF), ICHEP’96 Conference Proceedings.
- [23] Z. Kunszt and W. J. Stirling, “The LEP II W Mass Working Group Report”.